RSC Advances

PAPER

View Article Online
View Journal | View Issue

Cite this: *RSC Adv.*, 2021, **11**, 15296

High catalytic performance of Al–Pd–(Ru, Fe) icosahedral approximants for acetylene semi-hydrogenation†

Keishi Abe,[ab] Ryota Tsukuda,[ab] Nobuhisa Fujita [b] and Satoshi Kameoka *[b]

Received 12th March 2021
Accepted 14th April 2021

DOI: 10.1039/d1ra01958a

rsc.li/rsc-advances

Three cubic crystalline icosahedral approximants (C phase: $Al_{72.0}Pd_{16.4}Fe_{11.6}$, P_{40} phase: $Al_{72.0}Pd_{16.4}Ru_{11.6}$, P_{20} phase: $Al_{70.0}Pd_{22.3}Ru_{7.7}$) exhibit high ethylene selectivity of over 90% for hydrogenating acetylene at 150 °C. Moreover, the powdered P_{20} also demonstrates a high catalytic performance under an industry-like ethylene feed containing 0.5% acetylene as an impurity. Overall, icosahedral approximants in the Al–Pd–(Ru, Fe) systems are promising as a novel class of alloy catalysts.

1 Introduction

Intermetallic compounds (IMCs) exhibit a wide range of attractive functions and characteristics that are not attainable in ordinary elemental metals, such as a shape memory effect,[1] superconductivity.[2] and hydrogen absorption[3] They also possess excellent properties for hydrogenation catalysis, such as those demonstrated in Heusler alloys,[4,5] Zintl phases,[6] and hydrogen absorbing alloys.[3,7,8] Quasicrystals[9] are complex IMCs with aperiodic structures that often exhibit five-fold symmetry. Crystalline approximants, on the other hand, are periodic crystals having a similar chemical composition and atomic[10,11] and electronic structures[12] closely related to quasicrystals. The study of approximants is therefore crucial for understanding the structure and physical properties of quasicrystals. Despite earlier studies on quasicrystals as catalyst precursors,[13–15] there has been a recent awakening of interest in the ability of quasicrystals and approximants themselves to catalyze useful reactions at their terminated surfaces.

Recently, Kovnir and Armbrüster *et al.* demonstrated that GaPd, an IMC with a B20-type structure, is highly stable and selective for the semi-hydrogenation of acetylene to ethylene.[16,17] These authors proposed that the isolation of the catalytic element, Pd, in the Ga matrix as well as an alteration of the electronic structure due to alloying are the keys to the high catalytic performance. This assessment was soon extended to $Al_{13}Fe_4$ (ref. 18) and $Al_{13}Co_4$ (ref. 19) complex IMCs as noble-metal-free semi-hydrogenation catalysts. The fundamental processes in these catalytic reactions has been discussed based on the active site geometry on the surface.[20] as well as on the adsorption energies for the reactant molecules[21]

These studies revealed that the covalently bonded pentagonal $TMAl_5$ (TM = transition metal) complex on the surface provides active sites for both chemisorption of hydrocarbon species and dissociative adsorption of hydrogen,[20] and thus the specific surface structure plays a key role in the semi-hydrogenation of acetylene. The complex ensemble effect of $TMAl_5$ pentagons was also shown to be the origin of the activity for butadiene semi-hydrogenation.[21]

On the other hand, density functional theory (DFT) calculations demonstrated that the (210) surface of an AlPd (or GaPd) IMC with a B20-type crystal structure exposes active sites for the semi-hydrogenation of acetylene with extraordinarily high activity.[22,23] These active sites are associated with a triangular atomic configuration consisting of two Al (or Ga) atoms and one Pd atoms called a $PdAl_2$ triplet.

In fact, similar triplets may play a key role in the case of $Al_{13}TM_4$ because the $TMAl_5$ complex can be decomposed into five triangles each with two Al atoms and one TM atom, which is similar to the $PdAl_2$ triplet arrangement. Similar atomic configurations to $PdAl_2$ are frequently encountered in icosahedral quasicrystals and related approximants in Al–Pd–(Ru, Fe) systems. In other words, $PdAl_2$ triplets are involved in the atomic arrangements within the constituent clusters of these compounds.

Moreover, theory has shown that the selectivity for ethylene increases with increasing number of Ga atoms in the 1st coordination shell of each Pd atom,[24] and this trend probably also holds for Al–Pd. GaPd (or AlPd) which can be taken as the simplest analogue to the local atomic structure of icosahedral quasicrystals, and has at most four Ga (or Al) atoms adjacent to each Pd atom exposed on the surface. An Al–Pd–(Ru, Fe) approximant, on the other hand, can have up to five Al atoms surrounding the Pd atom, thus it is expected to show more prominent catalytic performance. To date, however, the

[a]*Department of Materials Processing, Graduate School of Engineering, Tohoku University, Sendai 980-8579, Japan*

[b]*Institute of Multidisciplinary Research for Advanced Materials, Tohoku University, Sendai 980-8577, Japan. E-mail: satoshi.kameoka.b4@tohoku.ac.jp*

† Electronic supplementary information (ESI) available. See DOI: 10.1039/d1ra01958a

catalytic performance of the Al–Pd–(Ru, Fe) approximants have rarely been investigated. We hereby present the first catalytic tests of three selected approximants in the Al–Pd–(Ru, Fe) systems for semi-hydrogenation of acetylene to experimentally demonstrate the high catalytic performance of these compounds. A possible origin of their catalytic properties is discussed in terms of their local atomic configurations.

2 Experimental

2.1 Samples

The samples used in this work were cubic crystalline approximants (C phase: $Al_{72.0}Pd_{16.4}Fe_{11.6}$, P_{40} phase: $Al_{72.0}Pd_{16.4}Ru_{11.6}$, P_{20} phase: $Al_{70.0}Pd_{22.3}Ru_{7.7}$) related to icosahedral quasicrystals. The pure Al, Pd, and Ru and/or Fe metals were melted in an argon atmosphere by using an arc furnace. Each ingot was typically of about 5 g. Parts of the ingot were annealed under an Ar atmosphere for up to 120 h (see Table S1 of ESI,† for annealing condition of all sample and see Section 1 of ESI,† for more details on sample preparation). The target approximant phases were confirmed by using powder X-ray diffraction (PXRD) patterns. Moreover, firmer evidence of the approximant phases was provided by selected area electron diffraction (SAED) patterns.

2.2 Catalytic test

The samples for catalytic test were prepared in a glove box under an Ar atmosphere to prevent surface oxidation. The samples were crushed in an agate mortar and sieved to size in the range of 25–75 μm. About 150 mg of fine-grained samples were packed in a quartz glass plug-flow reactor (inner diameter 7 mm) and plugged both ends by a ball bulb. The C_2H_2 hydrogenation tests were performed under a gas feed of 2% C_2H_2/80% H_2 in He, 0.1 MPa, with a flow rate of 30 mL min^{-1}. The hydrogenation under industrial like condition was performed with reaction gases 0.5% C_2H_2/49% C_2H_4/12.5% H_2 in He, 0.1 MPa, with a flow rate of 32 mL min^{-1} (see Section 3 of ESI,† for calculations of C_2H_4 selectivity and conversion).

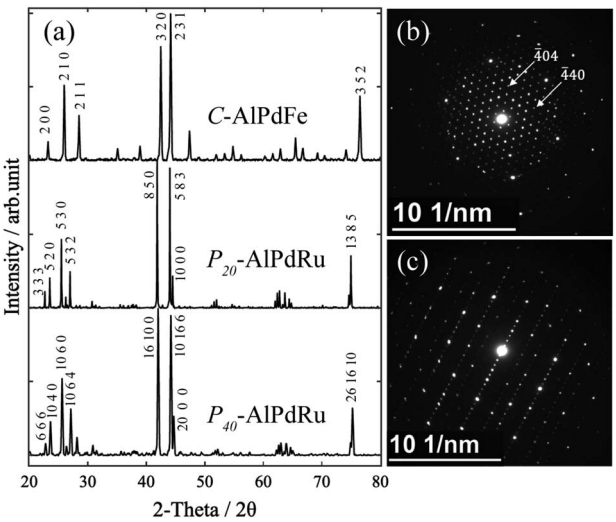

Fig. 1 (a) PXRD patterns for Al–Pd–(Ru, Fe) icosahedral approximants. (b and c) SAED patterns for P_{20}–AlPdRu phase, (b) [111], (c) pseudo five-fold zone axis.

3 Results and discussion

The PXRD patterns of C–AlPdFe, P_{20}–AlPdRu, and P_{40}–AlPdRu indexed as approximants were shown in Fig. 1(a). Fig. 1(b) and (c) show SAED patterns for the P_{20}–AlPdRu sample along three-fold and pseudo five-fold axes, respectively. In Fig. 1(b), the periodic array of spots can be indexed to a cubic crystal with a lattice constant of about 20 Å, as reported by Pavlyuchkov *et al.*[28]

The reaction rates ($mol_{C_2H_2}$ s^{-1} m^{-2}) for C_2H_2 and the C_2H_4 selectivity (%) are shown in Fig. 2(a) and (b), respectively. All three approximants showed a high ethylene selectivity of above 90% at 100 °C to 150 °C, and the P_{20}–AlPdRu specimen exhibited a maximum value of 98% at 150 °C. All approximants showed roughly the same selectivity, with all three having higher activity than $Al_{13}Fe_4$, which was reported to have high performance for semi-hydrogenation of C_2H_2, as shown in Fig. 2.

Assuming Langmuir–Hinshelwood (LH) mechanism on a catalytic cycle of the acetylene semi-hydrogenation reaction, reaction steps can be given as follows:

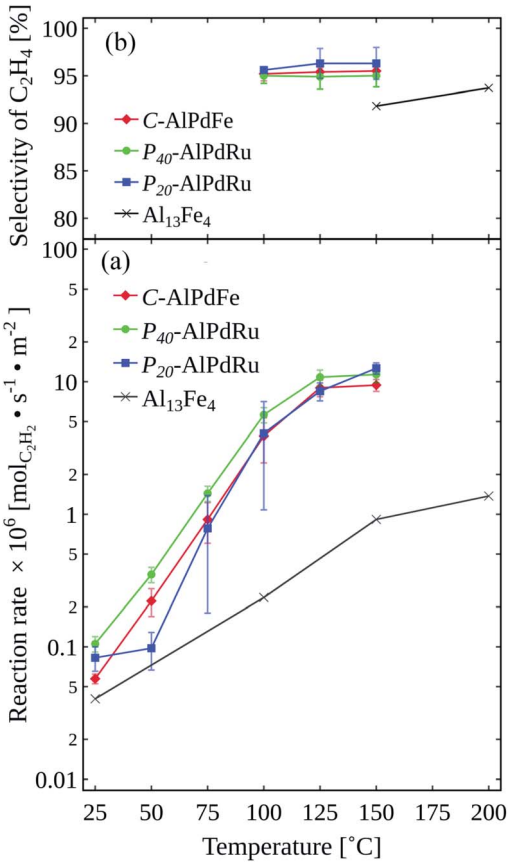

Fig. 2 (a) Reaction rate per surface area of catalyst and (b) selectivity for C_2H_4 over different Al–Pd–(Ru, Fe) icosahedral approximants and $Al_{13}Fe_4$ (reaction gas: 2.0% C_2H_2/80% H_2 in He; total pressure: 0.1 MPa; flow rate: 30 mL min^{-1}).

Step 1:

$$H_2 \rightarrow [H_2(a)] \rightarrow 2H(a)$$

Step 2:

$$C_2H_2 \rightarrow C_2H_2(a)$$

Step 3:

$$C_2H_2(a) + 2H(a) \rightarrow [C_2H_3(a) + H(a)] \rightarrow C_2H_4(a)$$

Step 4:

$$C_2H_4(a) \rightarrow C_2H_4$$

Step (1) and step (2) are the dissociative adsorption of H_2 and adsorption of C_2H_2 on the catalyst surface, respectively. Step (3) is the hydrogenation of $C_2H_2(a)$ to form $C_2H_x(a)$ ($x = 3$ or 4). Step (4) is the desorption of $C_2H_4(a)$ into gas phase as C_2H_4. Note here that an adsorbed state is represented by the symbol, (a).

Krajčí and Hafner identified catalytically active sites for C_2H_2 semi-hydrogenation in a $PdAl_2$ triplet exposed on the pseudo five-fold surface (//210) of B20-type AlPd.[22,23] According to their atomistic scenarios *via* LH mechanism, step (1) occurs on Pd sites that are slightly protruding towards the gas phase. Step (2) and step (3) proceed on $PdAl_2$ triplet sites that again involve a protruding Pd site. At step (2), C atoms in $C_2H_2(a)$ are di-σ bonded to two Al atoms in the Al–Al bridge position. At step (3), when an H atom is incorporated to from a CH_2 group, that end of the molecule is shifted towards and weakly bonded to the Pd atom whereas the bonding of the other end to the Al atom remain rather strong. After another H atom is incorporated, the C atoms are no longer bonded to the Al atoms, so that the molecule $C_2H_4(a)$ is only weakly π-bonded on top of the Pd atom. The desorption energy of $C_2H_4(a)$ is reportedly lower than the activation energy of ethylene to ethyl, so that ethylene desorbs at the final step.[22,23] As shown in Fig. 3(c) and (d), the present icosahedral approximants in the Al–Pd–(Ru, Fe) systems consist of mini-Bergman clusters (mBCs) and pseudo-Mackay clusters (pMCs).[27,29,30] We point out that many $PdAl_2$ triplets in Fig. 3(a) can be observed in the atomic arrangement of these clusters. For instance, five $PdAl_2$ triplets can be readily seen to form a $PdAl_5$ pentagon in the outer shell of pMCs (Fig. 3(b)), while other triplets can be found between the inner and outer shells of mBCs. Hence, the high activity and selectivity of the present approximants for the semi-hydrogenation of C_2H_2 could be attributed to the presence of similar triplets exposed on the surface.

A partial substitution of Ru with Fe in P_{20}–AlPdRu, or Fe with Ru in C–AlPdFe, caused little change in the reaction rate and selectivity, as shown in Section 3 of the ESI,† suggesting that the catalytic performance is generally insensitive to these elemental replacements between Fe and Ru. In other words, these elements seem to contribute much less to the catalytic activity

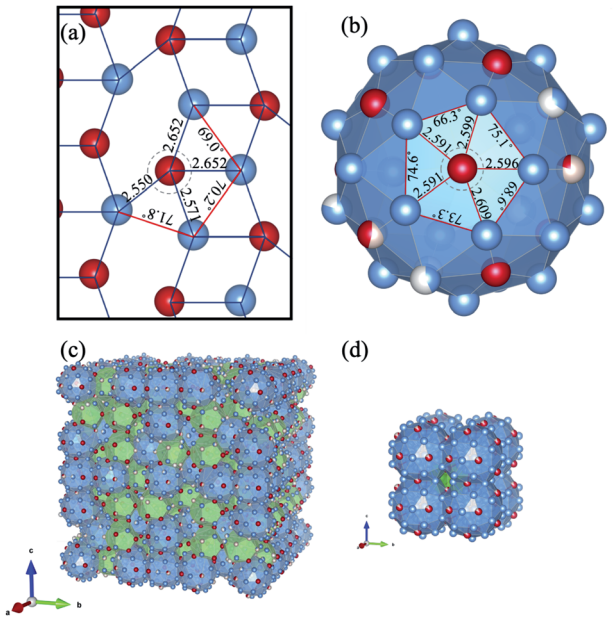

Fig. 3 (a) Triangles consisting of two Al atoms and one Pd atom in AlPd (210),[25] which are considered to be active for hydrogenation in the calculations. (b) Structure of pMCs constituting P_{40}–AlPdRu.[26] (c) Crystal structure of mBCs (shown as green polyhedrons) and pMCs (shown as blue polyhedrons) of P_{40}–AlPdRu.[26] Blue, Al; red, Pd; light pink, Ru. (d) Crystal structure of C–AlPdFe.[27].

than does Pd. In fact, the crystal structure appear to be much more essential in determining the catalytic properties. The simple binary IMCs, Al_3Pd_2 (trigonal, $P\bar{3}m1$) and Al_2Ru (orthorhombic, *Fddd*) (as detailed in Section 1 of the ESI,†), which are both similar in Al composition to the P_{20}–AlPdRu phase but are structurally much simpler, did not compete with the P_{20}–AlPdRu phase in the catalytic activity and selectivity (see Section 4 of the ESI,†). According to Krajčí *et al.*,[22,23] dissociation of hydrogen is possible only at transition metal atoms on the surface, but the Pd atoms need to be isolated because agglomerated transition metal atoms act as strong adsorbent for hydrogen and hydrocarbons, thereby reducing their mobility. Therefore, the high catalytic performance of the present approximants can be attributed to their complex crystal structures.

The specimens sieved under air did not show the high C_2H_4 selectivity (see Section 6 of the ESI,†). This is attributed to surface oxidation. Decomposition of the surface structure to Al_2O_3 and Pd by oxidation seems to trigger Pd aggregation, thus lowering the C_2H_4 selectivity. This is additional evidence that the surface structure is a key to the high catalytic performance.

The selective hydrogenation of C_2H_2 in the C_2H_4-rich gas is an important reaction for synthesizing polyethylene in the petrochemical industry,[31–33] an so we also examined the present samples under a more industry-like C_2H_4-rich gas feed. In Fig. 4, the catalytic performance of the present P_{20}–AlPdRu powder is compared with those of a commercial Lindlar catalyst and the $Al_{13}Fe_4$ powder under an industry-like C_2H_4-rich gas containing a 0.5% C_2H_2 impurity component (0.5% C_2H_2/49% C_2H_4/12.5% H_2 in He, 0.1 MPa, 32 mL min^{-1}). The P_{20}–AlPdRu phase sample

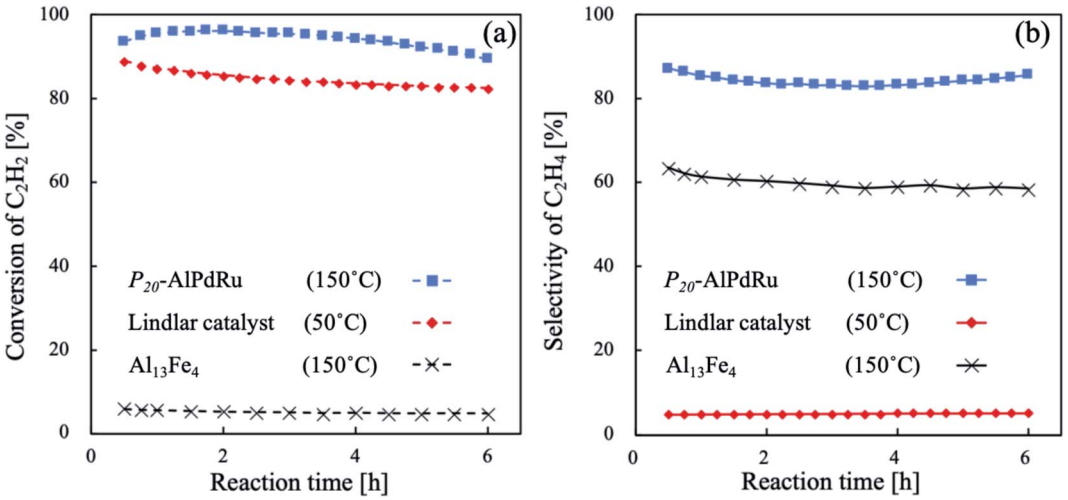

Fig. 4 (a) Conversion of C_2H_2 and (b) selectivity for C_2H_4 on P_{20}–AlPdRu, Lindlar catalyst and $Al_{13}Fe_4$ (reaction gas: 0.5% C_2H_2/49% C_2H_4/12.5% H_2 in He; total pressure: 0.1 MPa; flow rate: 32 mL min^{-1}).

again maintained a high conversion rate of over 80% along with a high ethylene selectivity of more than 83% (for detailed information on how to calculate the conversion and selection rates, see Section 3 of the ESI,†). P_{20}–AlPdRu showed higher selectivity than the commercial Lindlar catalyst and $Al_{13}Fe_4$.

A decrease in the conversion rate from the initial value of 92% was observed up to 6% after 6 h. This can be attributed to the deposition of carbon or higher hydrocarbons, referred to as green oil,[34] on the surface of the catalyst as indicated by a carbon-loss rate of about 10% throughout the reaction experiment. Still, it is important to note that the P_{20}–AlPdRu catalyst showed higher selectivity under industry-like conditions without specific optimization of the surface state such as coating with inert elements[35,36] or suppressing hydrogenation by CO gas.[37,38]

4 Conclusion

The quasicrystals and approximants are novel materials with many potential applications that are actively being explored, such as for low friction coefficients, high hardness, brittleness, and low thermal and electrical conductivity.[39] However, their crystal structures are often so complex that they are difficult to precisely determine. The structure of P_{20}–AlPdRu, for instance, has yet to be clarified, and those of C–AlPdFe[27] and P_{40}–AlPdRu[26] are still being argued. Nevertheless, recent crystallographic studies have revealed that their structures include common building blocks involving $PdAl_2$ triplets, which are the key to the semi-hydrogenation reaction. This study showed for the first time that high order Al–Pd–(Ru, Fe) approximants related to icosahedral Al–Pd–Mn quasicrystal are promising as alloy catalysts for the semi-hydrogenation of acetylene, and we expect to see further developments in this respect in the years to come.

Conflicts of interest

There are no conflicts to declare.

Acknowledgements

This work was financially supported by JSPS KAKENHI Grant No. JP19H05819 and JP19H05821.

Notes and references

1 *Shape memory alloys*, ed. H. Funakubo, Gordon and Breach Science Publishers, New York, 1987.
2 J. Nagamatsu, N. Nakagawa, T. Muranaka, Y. Zenitani and J. Akimitsu, *Nat*, 2001, **410**, 63–64.
3 R. Tsukuda, R. Yamagishi, S. Kameoka, C. Nishimura and A.-P. Tsai, *Sci. Technol. Adv. Mater.*, 2019, **20**, 774–785.
4 T. Kojima, S. Kameoka, S. Fujii, S. Ueda and A.-P. Tsai, *Sci. Adv.*, 2018, **4**, eaat6063.
5 T. Kojima, S. Kameoka and A.-P. Tsai, *ACS Omega*, 2019, **4**, 21666–21674.
6 K. L. Hodge and J. E. Goldberger, *J. Am. Chem. Soc.*, 2019, **141**, 19969–19972.
7 R. Tsukuda, T. Kojima, D. Okuyama, S. Kameoka, C. Nishimura and A.-P. Tsai, *Int. J. Hydrogen Energy*, 2020, **45**, 19226–19236.
8 K. Soga, H. Imamura and S. Ikeda, *J. Phys. Chem.*, 1977, **81**, 1762–1766.
9 D. Shechtman, I. Blech, D. Gratias and J. W. Cahn, *Phys. Rev. Lett.*, 1984, **53**, 1951–1953.
10 H. Takakura, C. P. Gómez, A. Yamamoto, M. De Boissieu and A. P. Tsai, *Nat. Mater.*, 2007, **6**, 58–63.
11 A. I. Goldman and R. F. Kelton, *Rev. Mod. Phys.*, 1993, **65**, 213–230.
12 T. Fujiwara and T. Yokokawa, *Phys. Rev. Lett.*, 1991, **66**, 333–336.
13 C. J. Jenks and P. A. Thiel, *J. Mol. Catal. A: Chem.*, 1998, **131**, 301–306.
14 A. Tsai and M. Yoshimura, *Appl. Catal., A*, 2001, **214**, 237–241.

15 B. P. Ngoc, C. Geantet, J. A. Dalmon, M. Aouine, G. Bergeret, P. Delichere, S. Raffy and S. Marlin, *Catal. Lett.*, 2009, **131**, 59–69.
16 K. Kovnir, M. Armbrüster, D. Teschner, T. Venkov, F. Jentoft, A. Knop-Gericke, Y. Grin and R. Schlögl, *Sci. Technol. Adv. Mater.*, 2007, **8**, 420–427.
17 M. Armbrüster, K. Kovnir, M. Behrens, D. Teschner, Y. Grin and R. Schlögl, *J. Am. Chem. Soc.*, 2010, **132**, 14745–14747.
18 M. Armbrüster, K. Kovnir, M. Friedrich, D. Teschner, G. Wowsnick, M. Hahne, P. Gille, L. Szentmiklósi, M. Feuerbacher, M. Heggen, F. Girgsdies, D. Rosenthal, R. Schlögl and Y. Grin, *Nat. Mater.*, 2012, **11**, 690–693.
19 M. Armbrüster, K. Kovnir, J. Grin, R. Schlogl, P. Gille, M. Heggen and M. Feuerbacher, *European Patent*, application No. 09157875A, 2009.
20 M. Krajčí and J. Hafner, *J. Catal.*, 2011, **278**, 200–207.
21 L. Piccolo, C. Chatelier, M.-C. De Weerd, F. Morfin, J. Ledieu, V. Fournée, P. Gille and E. Gaudry, *Sci. Technol. Adv. Mater.*, 2019, **20**, 557–567.
22 M. Krajčí and J. Hafner, *J. Phys. Chem. C*, 2012, **116**, 6307–6319.
23 J. Hafner and M. Krají, *Acc. Chem. Res.*, 2014, **47**, 3378–3384.
24 M. Krajčí and J. Hafner, *J. Phys. Chem. C*, 2014, **118**, 12285–12301.
25 P. Villars, L. D. Calvert and W. B. Pearson, *Pearson's handbook of crystallographic data for intermetallic phases*, American Society for Metals, Metals Park, Oh, 1985.
26 Y. Hatakeyama, N. Fujita and A. P. Tsai, *J. Phys.: Conf. Ser.*, 2017, **809**, 012007.
27 L. Hao and F. Changzeng, *Crystals*, 2019, **9**, 526.
28 D. Pavlyuchkov, B. Grushko and T. Velikanova, *J. Alloys Compd.*, 2009, **469**, 146–151.
29 R. Simura, K. Sugiyama, S. Suzuki and T. Kawamata, *Mater. Trans.*, 2017, **58**, 1101–1105.
30 N. Fujita, H. Takano, A. Yamamoto and A.-P. Tsai, *Acta Crystallogr., Sect. A: Found. Crystallogr.*, 2013, **69**, 322–340.
31 N. S. Schbib, M. A. García, C. E. Gígola and A. F. Errazu, *Ind. Eng. Chem. Res.*, 1996, **35**, 1496–1505.
32 A. Borodziński and G. C. Bond, *Catal. Rev.*, 2006, **48**, 91–144.
33 A. Borodziński and G. C. Bond, *Catal. Rev.*, 2008, **50**, 379–469.
34 A. Bos and K. Westerterp, *Chem. Eng. Process.*, 1993, **32**, 1–7.
35 H. Lindlar, *Helv. Chim. Acta*, 1952, **35**, 446–450.
36 W. Niu, Y. Gao, W. Zhang, N. Yan and X. Lu, *Angew. Chem., Int. Ed.*, 2015, **54**, 8271–8274.
37 D. Pope, *J. Catal.*, 1973, **28**, 46–53.
38 M. García-Mota, B. Bridier, J. Pérez-Ramírez and N. López, *J. Catal.*, 2010, **273**, 92–102.
39 J.-M. Dubois, *Chem. Soc. Rev.*, 2012, **41**, 6760–6777.